Photonic Generation of Multiform Microwave Frequency Shift Keying Signal

NA LI[1], GUODONG WANG [ID][2], KUISHENG FENG[1], XUAN LI [ID][2], WEI JIANG [ID][3], AND ZONGFENG LI[1]

[1]College of Artificial Intelligence, Yango University, Fuzhou 350015, China
[2]College of Information and Navigation, Air Force Engineering University, Xi'an 710077, China
[3]National Key Laboratory of Science and Technology on Space Microwave, Xi'an 710000, China

Corresponding author: Guodong Wang (1535859250@qq.com)

ABSTRACT A photonic approach to generate multiform microwave frequency shift keying (FSK) signal is proposed. In the scheme, a dual-polarization quadrature phase shift-keying (DP-QPSK) modulator along with a polarization controller (PC) is employed to generate two orthogonally polarized signals containing specific optical sidebands, and a following tunable filtering switch (TFS) serve as optical sidebands selector. From a theoretical analysis, when the modulators in the scheme are properly biased, we can obtain microwave FSK signal with frequency multiplication factors of 2/4 or microwave FSK signal with flexible tunable subcarrier frequencies. Simulations are conducted to verify the proposed scheme. 10/20GHz and 8/12GHz microwave FSK signals are successfully generated, and the frequency tunability is also demonstrated. In addition, the impact of the non-ideal parameters is analyzed, and the results show that the scheme has good immunity to the small parameters deviation (within 3°). The distinct advantage of our scheme is that we realize multiform microwave FSK signal generation based on a single system, which may find applications in high-frequency multifunction wireless communication system or radar system.

INDEX TERMS Microwave photonics, microwave signal generation, frequency shift keying.

I. INTRODUCTION

Microwave frequency shift keying (FSK) signal, featuring strong anti-jamming ability and anti-interception ability, has been widely used in wireless communication, radar, electronic warfare systems [1], [2]. Traditionally, the generation method of microwave FSK signal is based on electronic devices in the electrical domain, resulting in the limited operating frequency, small tunability and low bit-rate due to the well-known electronic bottleneck.

Compared to its electrical counterparts, photonic generation of microwave FSK signal has many advantages including broad bandwidth, low loss, large tunability and immunity to electromagnetic interference [3], [4]. So far, various photonic solutions to generate microwave FSK signal have been proposed. These microwave FSK signals usually can be classified into two forms. One is that the subcarriers of

the microwave FSK signal have a fixed multiple relationship [5]–[7], and the other is that the subcarriers can be tuned flexibly [8]–[14].

In [5] and [6], the binary coding signal is sent into a Mach-Zehnder modulator (MZM) to switch the bias point between quadrature transmission point (QTP) and minimum transmission point (MITP), then a microwave FSK signal can be obtained after photodetection, and its two subcarriers are respectively the fundamental and doubling frequency of the input RF signal, which can be also understood that the two subcarriers have frequency multiplication factors (FMF) of 1 and 2. Therefore, we express the obtained signal as the microwave FSK signal with FMF of 1/2. To increase the FMF, a cascaded structure containing a dual-polarization quadrature phase shift keying (DP-QPSK) modulator and a polarization modulator (PolM) is proposed in [7]. Two double-sideband (DSB) modulated signals with orthogonal polarization states are output from DP-QPSK modulator, and then experience complementary phase modulations in the

PolM driven by a binary coding signal. Finally, a microwave FSK signal with FMF of 4/8 can be obtained after photodetection. The advantage of this form of microwave FSK signal is that high-frequency subcarriers can be obtained through the low-frequency RF input signal and the operating bandwidth is very large, making it suitable for sophisticated electronic warfare systems. However, the fixed multiple relationship between the subcarriers may limit its applications for some scenarios, where more flexible subcarriers is highly desired.

In [8]–[10], the polarization direction of optical carrier is switched by a PolM and then inject into a polarization-dependent parallel structure, in which two MZMs are placed in parallel. By adjusting the two MZMs to work at the MITP, microwave FSK signal can be obtained. In [11] and [12], only a polarization-division-multiplexed MZM is used to generate microwave FSK signal by adjusting the bias point of two MZMs to switch between QTP and MITP. In [13], a PolM also acts as a polarization switch, and a polarization maintaining fiber Bragg grating (PM-FBG) is employed to select different optical sideband in different polarization directions, then the output optical sideband is combined with a tunable optical source and sent into a photodetector (PD) to generate microwave FSK signal. In [14], a traveling-wave silicon modulator is designed to act as a tunable filtering switch (TFS). In the scheme, one of two DSB modulated optical signals is selected by the TFS, which is controlled by a binary coding signal, and then microwave FSK signal can be obtained after photodetection. The above schemes can obtain microwave FSK signals with flexibly tunable subcarriers, but two radio frequency (RF) input signals or an additional tunable optical source are required, and the FMF can only reach 2.

In this paper, we propose a photonic approach to generate the aforementioned two forms of microwave FSK signals based on a single system, which is mainly contains a DP-QPSK modulator and a TFS. By adjusting the RF driving signals and the DC bias voltages of the DP-QPSK modulator, its output signal will contain specific optical sidebands. And the TFS serves as optical sidebands selector. Microwave FSK signal with FMF of 2/4 and microwave FSK signal with flexible tunable subcarrier frequencies are generated in this system. Besides, the system has good immunity to the deviation of non-ideal parameters. The distinct advantage of our scheme is that we realize multiform microwave FSK signal generation based on a single system, making up for the shortcomings of either of these two forms of microwave FSK signal, enabling the scheme to accommodate more flexible applications.

II. THEORY AND PRINCIPLE

The schematic diagram of the proposed multiform microwave FSK signal generator is shown in Fig. 1. In the scheme, an optical carrier from a laser diode (LD) is sent into a DP-QPSK modulator. The DP-QPSK modulator contains two dual-parallel MZM (DPMZM), a 90° polarization rotator (PR) and a polarization beam combiner (PBC), which can be seen in Fig. 2. With the joint use of the followed polarization
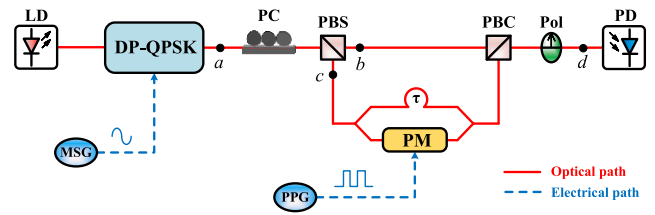

FIGURE 1. Schematic diagram of the proposed multiform microwave FSK signal generator. LD: laser diode. MSG: microwave signal generator. DP-QPSK: dual-polarization quadrature phase shift keying. PC: polarization controller. PBS: polarization beam splitter. PM: phase modulator. PPG: pulse pattern generator. PBC: polarization beam combiner. Pol: polarizer. PD: photodetector.

controller (PC) and polarization beam splitter (PBS), the output signal of the DP-QPSK modulator will be polarization separated into two paths, then one of the two paths enters the TFS and undergoes sideband selection. The TFS is a parallel structure in which the upper arm contains an optical tunable delay line (OTDL) and the lower one contains a phase modulator (PM). Finally, the two paths optical signal are recombined and inject into a PD for photodetection. As a result, by adjusting the RF input signals, DC bias of the DP-QPSK modulator and the optical delay of the OTDL, two forms of microwave FSK signals can be obtained.

A. FSK WITH FMF OF 2/4

Fig. 2 shows the configuration of DP-QPSK modulator for the generation of microwave FSK signal with FMF of 2/4. The RF driving signal from a microwave signal generator (MSG) is divided into two parts, one part sent into MZM_1 directly and the other part sent into MZM_4 after 45° phase shift. The remaining two RF ports of MZM_2 and MZM_3 are empty. The bias voltages are adjusted to make $\varphi_1 = \varphi_4 = 0°$, $\varphi_3 = 180°$. Meanwhile, φ_2 is adjusted to make the amplitude of the optical carrier output from MZM_2 $\sqrt{2}$ times to the optical carrier output from MZM_1. Supposing that the expression of the RF driving signal is $V_r \sin(\omega_r t)$, where V_r and ω_r are respectively the amplitude and angular frequency. Then the output signals of MZM_i ($i = 1,2,3,4$) can be expressed as[15]:

$$E_1 = \frac{E_{in}(t)}{2}\left(J_0(m) + J_2(m)\,e^{j2\omega_r t} + J_2(m)\,e^{-j2\omega_r t}\right) \quad (1)$$

$$E_2 = \frac{E_{in}(t)}{2}\cos(\frac{\varphi_2}{2}) = \frac{\sqrt{2}E_{in}(t)}{2}J_0(m) \quad (2)$$

$$E_3 = \frac{E_{in}(t)}{2}\cos(\frac{\varphi_3}{2}) = 0 \quad (3)$$

$$E_4 = \frac{E_{in}(t)}{2}\left(J_0(m)+J_2(m)\,e^{j2\omega_r t+\pi/2} + J_2(m)\,e^{-j2\omega_r t-\pi/2}\right) \quad (4)$$

where $E_{in}(t)$ is the output of LD. m represents the modulation index and equals to $\pi V_r/V_\pi$, V_π is the half-wave voltage of the MZMs. α and β are respectively the bias phase of MZM_2 and MZM_3. J_n denotes the nth-order Bessel function of the first kind. It should be noted that the optical sidebands with orders higher than 2 are ignored for the sake of low power.
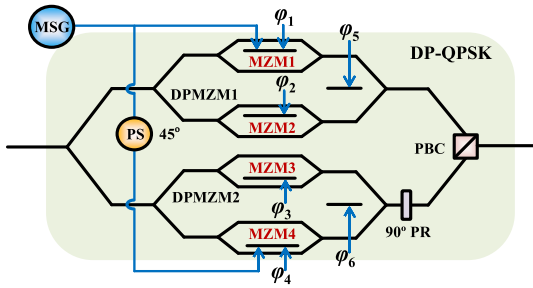
FIGURE 2. The configuration of DP-QPSK modulator for the generation of microwave FSK signal with FMF of 2/4. PS: phase shifter. PR: polarization rotator.

The main bias voltages of the $DPMZM_1$ and $DPMZM_2$ are respectively tuned to introduce a phase shift of 135° and 90°, i.e., $\varphi_5 = 135°$ and $\varphi_6 = 90°$. Thus, the output of the DP-QPSK modulator can be written as:

$$
\begin{aligned}
&E_{DP\text{-}QPSK} \\
&= \begin{bmatrix} E_{DPMZM1} \\ E_{DPMZM2} \end{bmatrix} = \frac{\sqrt{2}}{2} \begin{bmatrix} E_1 + E_2 e^{j3\pi/4} \\ E_3 + E_4 e^{j\pi/2} \end{bmatrix} \\
&= \frac{E_{in}(t)}{2\sqrt{2}} \begin{bmatrix} J_0(m)e^{j\pi/2} + J_2(m)\,e^{j2\omega_r t} + J_2(m)\,e^{-j2\omega_r t} \\ J_0(m)e^{j\pi/2} + J_2(m)\,e^{j2\omega_r t+j\pi} + J_2(m)\,e^{-j2\omega_r t} \end{bmatrix}
\end{aligned}
\tag{5}
$$

From Eq. (5), we can see that the optical carriers and −2nd-order sidebands in two polarization states are in phase while the +2nd-order sidebands are out of phase. Therefore, when PC is adjusted to rotate the polarization direction of the signal to have an angle of 45? with respect to the principle axis of the PBS, the two outputs of the PBS (PBS-x and PBS-y) are as follows:

$$
\begin{aligned}
E_{PBS} &= \begin{bmatrix} E_{PBS-x} \\ E_{PBS-y} \end{bmatrix} = \frac{\sqrt{2}}{2} \begin{bmatrix} E_{DPMZM1} - E_{DPMZM2} \\ E_{DPMZM1} + E_{DPMZM2} \end{bmatrix} \\
&= \frac{E_{in}(t)}{4} \begin{bmatrix} J_2(m)\,e^{j2\omega_r t} \\ J_0(m)e^{j\pi/2} + J_2(m)\,e^{-j2\omega_r t} \end{bmatrix}
\end{aligned}
\tag{6}
$$

As can be seen, the +2nd-order sideband is polarization separated from the optical carrier and the −2nd-order sideband. After that, the optical carrier and the −2nd-order sideband are routed to the TFS, which has a frequency response as below:

$$
H(\omega) = \frac{1}{2}(e^{j\theta} + e^{-j\omega\tau}) = e^{j(\theta - \omega\tau)/2} \cos\left(\frac{\theta + \omega\tau}{2}\right) \tag{7}
$$

where $\theta = \pi s(t)/V_{PM}$ represents the phase shift introduced by the PM, $s(t)$ is the binary coding signal generated by a pulse pattern generator (PPG), V_{PM} is the half-wave voltage of the PM. τ denotes the time delay between the two parallel paths which can be tuned by the OTDL. It should be noted that we did not consider the attenuations of the two paths to simplify the analysis. In practical applications, when proper device (such as *kylia* WT-MINT) is used to perform the function of the TFS, an adjustable attenuator embedded in one path can balance the optical power between the two paths.

Assuming that the $E_{in}(t) = \exp(j\omega_c t)$, where ω_c is the angular frequency of optical carrier, then the output of TFS can be written as:

$$
E_{TFS} = \frac{e^{j\omega_c t}}{4} \begin{pmatrix} J_0(m)e^{j(\frac{\pi}{2}+\frac{\theta}{2}-\frac{\omega_c\tau}{2})}\cos(\frac{\theta}{2}+\frac{\omega_c\tau}{2}) \\ +J_2(m)\,e^{j(-2\omega_r t+\omega_r\tau+\frac{\theta}{2}-\frac{\omega_c\tau}{2})} \\ \cos(\frac{\theta}{2}+\frac{\omega_c\tau}{2}-\omega_r\tau) \end{pmatrix} \tag{8}
$$

For simplify, we assume that $\omega_c\tau/2 = 2k\pi$, k is equal to an integer. It should be noted that even if $\omega_c\tau/2 \neq 2k\pi$, we can compensate for it by adding a bias $\Delta\theta$ to the amplitude of $s(t)$ to realize $\omega_c\tau/2 + \Delta\theta = 2k\pi$. Therefore, we default $\omega_c\tau/2 = 2k\pi$. Setting the time delay τ to satisfy $\omega_r\tau = \pi/2$, and adjusting the amplitude of $s(t)$ to make $\theta = \pi$ when $s(t)$ is bit '0' and $\theta = 0$ when $s(t)$ is bit '1'. As a result, Eq. (8) can be rewritten as:

$$
E_{TFS} = \begin{cases} \dfrac{J_2(m)}{4}e^{j(\omega_c-2\omega_r)t+j\pi} & for\ s(t) = bit'0' \\[2mm] \dfrac{J_0(m)}{4}e^{j\omega_c t+j\pi/2} & for\ s(t) = bit'1' \end{cases} \tag{9}
$$

The output of TFS will recombine with the +2nd-order sideband by a polarization beam combiner (PBC) and a polarizer, and undergo optical to electrical conversion in the PD, we obtain:

$$
I_{AC} \propto \begin{cases} J_2^2(m)\cos(4\omega_r t - \pi) & for\ s(t) = bit'0' \\ J_0(m)J_2(m)\cos(2\omega_r t - \pi/2) & for\ s(t) = bit'1' \end{cases} \tag{10}
$$

As can be seen, a microwave FSK signal is obtained with frequency multiplication factors of four for bit '0' and two for bit '1', respectively. Note that when the modulation index m is adjusted to 1.841, $J_0(m) = J_2(m)$, the two subcarrier frequencies of the FSK signal have uniform amplitude. Fig. 3 depicts the schematic diagram of the spectra at the output of different devices, in which the output of DP-QPSK modulator corresponds to point a in Fig. 1, the output of PBS corresponds to point b and c in Fig. 1, and the output of Pol corresponds to point d in Fig. 1.

B. FSK WITH TUNABLE SUBCARRIER FREQUENCIES

Fig. 4 shows the configuration of the DP-QPSK modulator for the generation of microwave FSK signal with tunable subcarrier frequencies. The RF driving signal is divided into two parts, one part sent into MZM_1 after 90° phase shift and the other part sent into MZM_2 directly, the bias voltages are adjusted to make $\varphi_1 = \varphi_2 = 180°$, $\varphi_5 = -90°$. This way, the obtained optical signal output from $DPMZM_1$ mainly contains the −1nd-order sideband [16]. Another RF driving signal is also divided into two parts, one part sent into MZM_3 directly and the other part sent into MZM_4 after 90° phase shift, the bias voltages are adjusted to make $\varphi_3 = \varphi_4 = 0°$, $\varphi_6 = 180°$, then the obtained optical signal output from $DPMZM_2$ mainly contains the ±2nd-order sidebands [17]. Supposing that the expression of the two RF driving signals
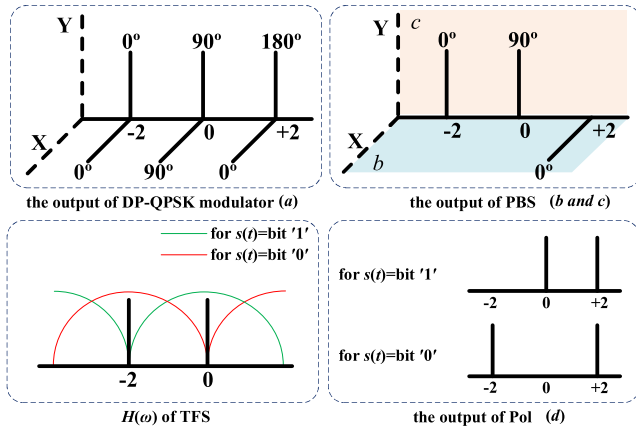
FIGURE 3. The schematic diagram of the spectra at the output of different devices (DP-QPSK modulator, PBS and Pol) and the $H(\omega)$ of TFS.
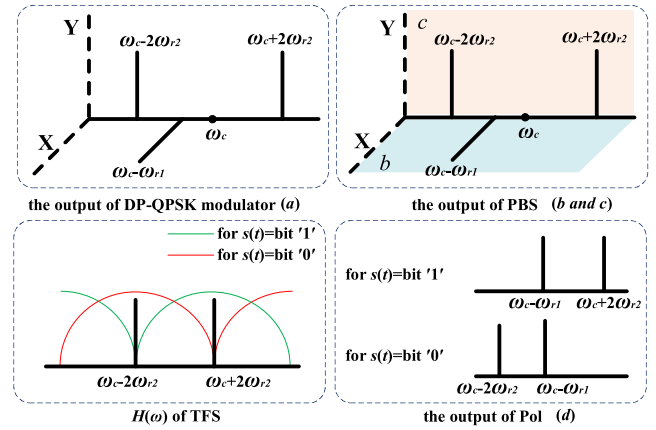

FIGURE 5. The schematic diagram of the spectra at the output of different devices (DP-QPSK modulator, PBS and Pol) and the $H(\omega)$ of TFS.
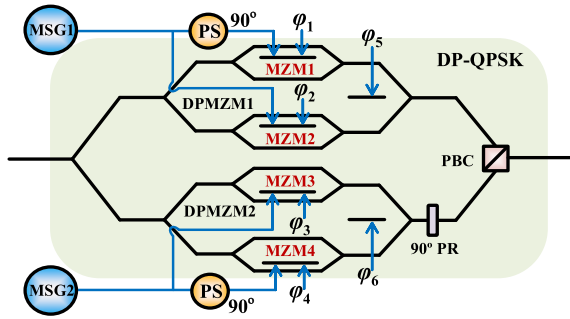

FIGURE 4. The configuration of DP-QPSK modulator for the generation of microwave FSK signal with tunable subcarrier frequencies.

are $V_{r1}\sin(\omega_{r1}t)$ and $V_{r2}\sin(\omega_{r2}t)$, respectively. Then the output of the DP-QPSK modulator can be expressed as:

$$
E_{\text{DP-QPSK}} = \begin{bmatrix} E_{\text{DPMZM1}} \\ E_{\text{DPMZM2}} \end{bmatrix}
$$
$$
= \frac{E_{in}(t)}{2\sqrt{2}} \begin{bmatrix} J_1(m_1)\,e^{-j\omega_{r1}t+j\pi} \\ J_2(m_2)\,e^{j2\omega_{r2}t} + J_2(m_2)\,e^{-j2\omega_{r2}t} \end{bmatrix}
\tag{11}
$$

where m_i ($i = 1,2$) denotes the modulation index and equals to $\pi V_{ri}/V_\pi$. The followed PC is adjusted to rotate the polarization direction of the signal to align with the principle axis of the PBS. As a result, the E_{DPMZM1} and E_{DPMZM2} are respectively output from the two ports of the PBS and the E_{DPMZM2} will route to the TFS. According to Eq. (7), the output of TFS can be written as:

$$
E_{\text{TFS}} = \frac{e^{j\omega_c t}}{2\sqrt{2}} \left(\begin{array}{l} J_2(m_2)e^{j(2\omega_{r2}t-\omega_{r2}\tau+\theta/2)}\cos(\frac{\theta}{2}+\omega_{r2}\tau) \\ +J_2(m_2)\,e^{j(-2\omega_{r2}t+\omega_{r2}\tau+\theta/2)}\cos(\frac{\theta}{2}-\omega_{r2}\tau) \end{array} \right)
\tag{12}
$$

Setting the time delay τ to satisfy $\omega_{r2}\tau = \pi/4$, and adjusting the amplitude of $s(t)$ to make $\theta = \pi/2$ when $s(t)$ is bit '0' and $\theta = -\pi/2$ when $s(t)$ is bit '1'. Then Eq. (12)

can be rewritten as:

$$
E_{\text{TFS}} = \begin{cases} \dfrac{J_2(m_2)}{2\sqrt{2}}e^{j(\omega_c-2\omega_{r2})t+j\pi/2} & for\ s(t) = bit\,'0' \\[2mm] \dfrac{J_2(m_2)}{2\sqrt{2}}e^{j(\omega_c+2\omega_{r2})t-j\pi/2} & for\ s(t) = bit\,'1' \end{cases}
\tag{13}
$$

After the PBC and the polarizer, the output of TFS will recombine with the E_{DPMZM1} and undergo photoelectric conversion in the PD, we obtain:

$$
I_{\text{AC}} \propto \begin{cases} \cos(\left|2\omega_{r2}-\omega_{r1}\right|t-\dfrac{\pi}{2}) & for\ s(t) = bit\,'0' \\[2mm] \cos(\left|2\omega_{r2}+\omega_{r1}\right|t+\dfrac{\pi}{2}) & for\ s(t) = bit\,'1' \end{cases}
\tag{14}
$$

It can be found from Eq. (14) that a microwave FSK signal with two subcarrier frequencies $\left|2\omega_{r2}-\omega_{r1}\right|$ and $\left|2\omega_{r2}+\omega_{r1}\right|$ is successfully generated. Supposing that a microwave FSK signal with two subcarriers of 30GHz and 32GHz is wanted for millimeter wave communication, our scheme can set $\omega_{r1} = 1$GHz and $\omega_{r2} = 15.5$GHz, which indicates that we only need a low-frequency RF input and a high-frequency RF input to generate the high-frequency microwave FSK signal, and the two subcarrier frequencies can be continuously tuned by adjusting the low frequency RF input ω_{r1}. In contrast, the schemes in [11] and [12] need two RF inputs at 15GHz and 16GHz to achieve the same task, which increases the requirements for RF sources. Fig. 5 depicts the schematic diagram of the spectra at the output of different devices.

III. SIMULATION RESULTS AND DISCUSSION
A simulation system based on Fig.1 is built up to verify the performance of the proposed scheme. The adopted parameters of the system are set according to actual device parameters which are listed in Table.1. The MSG[1] is employed in the generation process of microwave FSK signal with FMF of 2/4, and the MSG[2] is employed in the generation process of microwave FSK signal with flexible tunable subcarrier frequencies.

When it comes to the generation of microwave FSK signal with FMF of 2/4, the DP-QPSK modulator is configured as

Device	Parameters
Laser	*Frequency: 193.1 THz*
	Power: 16 dBm
	Linewidth: 10 MHz
MZM	*Extinction Ratio: 30 dB*
	half-wave Voltage: 4 V
	Insertion Loss: 5 dB
MSG$^{(1)}$	*Frequency: 5 GHz*
	Amplitude: 2.34 V
MSG$^{(2)}$	*Frequency: 2 GHz and 5 GHz*
	Amplitude: 1 V
PD	*Responsivity: 1 A/W*
PPG	*Rise/Fall time: 0.05 bit*

shown in Fig. 2. The frequency of the RF driving signal is set to 5GHz and the amplitude is set to satisfy $m = 1.841$. Since the outputs of DPMZM$_1$ and DPMZM$_2$ have the same optical spectrum, only one of them is shown in Fig. 6(a). As can be seen, the optical carrier and $\pm$2nd-order sidebands are retained and have identical amplitude. In addition, the optical spurious suppression ratio (OSSR) is 25.11dB so that the influence of undesired sidebands can be ignored due to their much lower power than that of the desired sidebands. The rotation angle of PC is set to 45°. Fig. 6(b) shows the spectra at the output of PBS, in which the optical carrier and the $-$2nd-order sidebands (red color) are output from the y port of PBS while the +2nd-order sideband (blue color) is output from the x port. The results are consistent with the theoretical analysis.
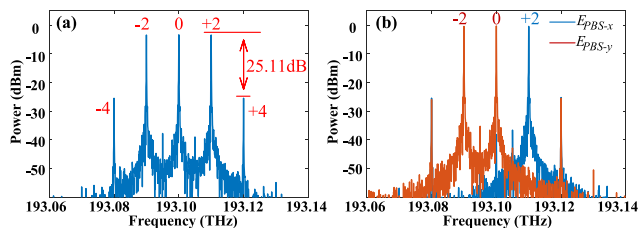

FIGURE 6. The spectra at the output of (a) DPMZMs and (b) PBS.

The optical carrier and the $-$2nd-order sideband are then routed to the TFS. The time delay τ is adjusted to 50ps to satisfy $\omega_r \tau = \pi/2$. When the binary coding signal is bit '1', its amplitude is set to 0V, then the frequency response of TFS is shown as the green line in Fig. 7(a). And when the binary coding signal is bit '0', its amplitude is set to 4V, then the frequency response of TFS is shown as the red line in Fig. 7(a). Fig. 7(b) shows the optical spectrum at the output of the TFS in the cases that the binary coding signal is all bit '1' (red line) or all bit '0' (blue line). As can be seen, the $-$2nd-order sideband is filtered and the optical carrier is retained with an OSSR of 25.10dB when binary coding signal is all bit '1'. Conversely, the optical carrier is filtered and the $-$2nd-order sideband is retained with an OSSR of 38.91dB when binary coding signal is all bit '0'.
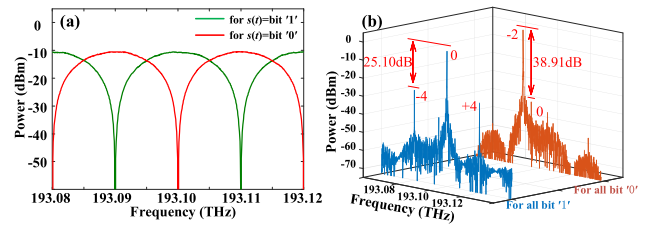

FIGURE 7. (a) the frequency response and (b) the output optical spectrum of TFS.

Finally, the binary coding signal is set to have a pattern of "010011" with a bit rate of 1-Gbit/s, then we obtain a microwave FSK signal at the output of PD. In Fig. 8(a), the electrical spectrum of the generated FSK signal is shown and there are two subcarrier frequencies at 10GHz and 20GHz, indicating that the frequency multiplication of 2/4 is successfully implemented. Besides, the power of the two spectral components is more than 24.62dB higher than other spurious spectral components, which means that the generated microwave FSK signal has high electrical spectrum purity. Fig. 8(b) shows the waveform of the generated 1-Gbit/s 10/20GHz microwave FSK signal, in which the frequency jump can be clearly observed and the recovered binary data (red line) obtained by coherent demodulation is also shown. It is noticed that the curve of recovered binary data is consistent with the binary coding signal.
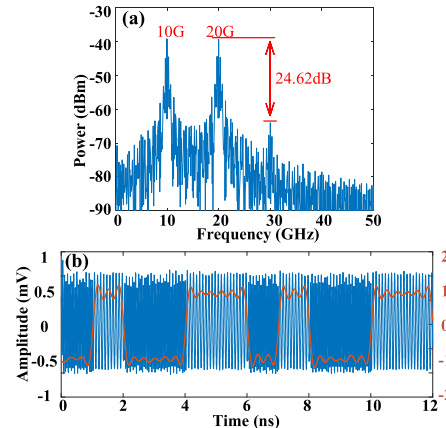

FIGURE 8. (a) the electrical spectrum and (b) the waveform of the generated 1-Gbit/s 10/20 GHz microwave FSK signal.

On the other hand, when it comes to the generation of microwave FSK signal with flexible tunable subcarrier frequencies, the DP-QPSK modulator is configured as shown in Fig.4. The frequency and amplitude of MSG1 are respectively set to 2GHz and 1V, then the output optical spectrum of DPMZM$_1$ is shown in Fig. 9(a), in which the $-$1st-order sidebands are retained with an OSSR of 30.29dB. The frequency and amplitude of MSG2 are respectively set to 5GHz and 4V, then the output optical spectrum of DPMZM$_2$ is shown in Fig. 9(b), in which the $\pm$2st-order sidebands are retained with an OSSR of 37.77dB. The rotation angle of PC is set to 0°. Therefore, the signal in Fig. 9(a) is output from the
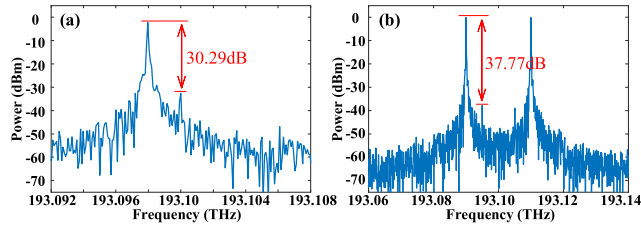
FIGURE 9. The output optical spectrum of (a) DPMZM$_1$ and (b) DPMZM$_2$.

x port of PBS while the signal in Fig. 9(b) is output from the *y* port, and then routed to the TFS.

The time delay τ of the TFS is adjusted to 25ps to satisfy $\omega_{r2}\tau = \pi/4$. The amplitude of the binary coding signal is set to 2V for bit '0' and −2V for bit '1', then the frequency response of TFS is shown in Fig. 10(a). Fig. 10(b) shows the optical spectrum at the output of the TFS in the cases that the binary coding signal is all bit '1' (red line) or all bit '0' (blue line). As can be seen, the +2st-order sideband is retained with an OSSR of 37.45dB when binary coding signal is all bit '1', conversely, the −2nd-order sideband is retained with an OSSR of 36.92dB when binary coding signal is all bit '0'.
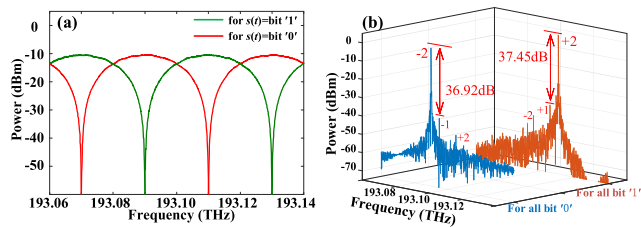

FIGURE 10. (a) The frequency response and (b) the output optical spectrum of the TFS.

Similarly, the binary coding signal is also set to have a pattern of "010011" with a bit rate of 1-Gbit/s, then we obtain a microwave FSK signal at the output of PD, whose electrical spectrum and waveform are respectively shown in Fig. 11(a) and (b). As can be seen, the two subcarrier frequencies satisfy $|2 \times 5\pm2|$GHz, which agrees well with the conclusion in Eq. (13). In addition, the RF spurious suppression ratio (RFSSR) can reach 22.69dB, which means high purity of the electrical spectrum.

It is worth mentioned that the two subcarrier frequencies can be tuned flexibly. For example, when we adjust the frequency of MSG1 from 2GHz to 6GHz by 1GHz steps, the instantaneous frequency of the generated microwave FSK signal is shown in Fig. 12, which is obtained by Hilbert transform. As can be seen, the two subcarrier frequencies are respectively equal to 4/16GHz, 5/15GHz, 6/14GHz and 7/13GHz as the frequency of the MSG1 changes.

The aforementioned theoretical analysis and simulation results show that two forms of the microwave FSK signal can be successfully generated, enabling the scheme to accommodate more flexible applications. This is mainly benefit from the joint use of DPQPSK modulator, PC and PBS. DP-QPSK modulator is widely used in microwave signal generation [18]
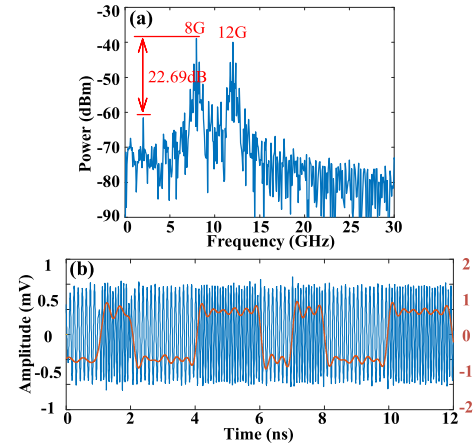

FIGURE 11. (a) The electrical spectrum and (b) the waveform of the generated 1-Gbit/s 8/12 GHz microwave FSK signal.
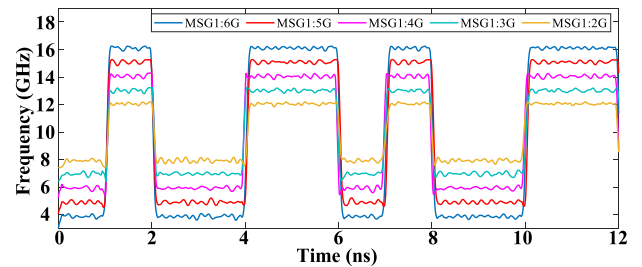

FIGURE 12. The instantaneous frequency of the generated microwave FSK signal at MSG1 frequency of 2/3/4/5/6 GHz.

and [19], frequency conversion [20] and other fields since it can perform many different functions due to the rich RF and DC interfaces. In [18], all four sub-MZMs of DPQPSK modulator are set to generate even-order optical sidebands. In [19], the DC biases of DPQPSK modulator is carefully adjusted to control the power ratio between each optical sideband, so as to realize the generation of triangular wave or square wave. In [20], both the two DP-MZMs of DPQPSK modulator are set to generate ±1st optical sidebands. While in our scheme, the DP-QPSK modulator is employed to generate two orthogonally polarized signals containing specific optical sidebands, which are then polarization separated into two paths with the joint use of PC and PBS. Finally, the TFS controlled by a binary coding signal serve as optical sidebands selector to filter out the unwanted sideband of one path. With their cooperation, we can perform the generation of two forms microwave FSK signals.

It should be pointed out that there are various non-ideal factors in the actual experimental environment, which lead to the deviation of the parameters from theoretical value, such as the phase value of the PS, the rotate angle of PC and the DC bias, thus resulting in the deterioration of the signal quality. Due to the limited experimental conditions, we cannot carry out experimental verification for the time being. Therefore, taking the generation of microwave FSK signal with a tunable subcarrier frequency as an example,

we will discuss the impact of non-ideal parameters on the signal quality through simulation analysis.

Fig.13 (a) shows the impact of non-ideal phase shift on the OSSR of the output spectrum of $DPMZM_1$ (blue color) and $DPMZM_2$ (red color). Fig.13 (b) and Fig.13 (c) respectively show the output optical spectrum of $DPMZM_1$ and $DPMZM_2$ when the phase deviation is 3°. As can be seen, the non-ideal phase shift increases the power of higher-order spurious sideband components (green circle). However, these spurious sideband components are still not the one with the maximum power when the phase shift deviation is less than 3°, so they have little effect on the OSSR of the output spectrum of two DPMZMs.
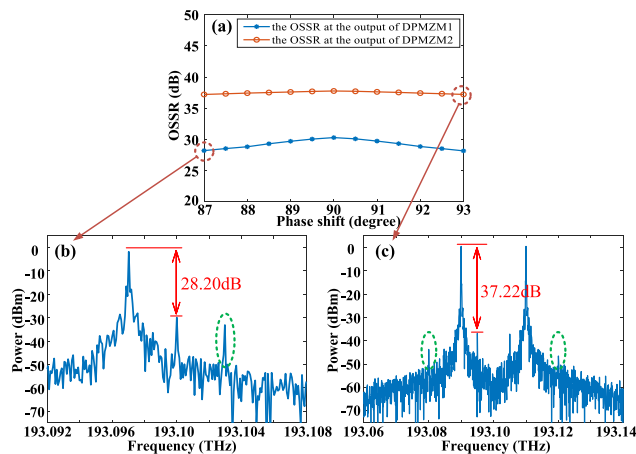

FIGURE 13. (a) the OSSR of the output spectrum of two DPMZMs when phase deviation is within 3°. (b) the output optical spectrum of $DPMZM_1$ when the phase shift is 87°. (c) the output optical spectrum of $DPMZM_2$ when the phase shift is 93°.

Fig.14 (a) shows the impact of non-ideal rotate angle on the OSSR of the output spectrum at PBS-*x* (blue color) and PBS-*y* (red color). Fig.14 (b) and Fig.14 (c) respectively show the output optical spectrum at PBS-*x* and PBS-*y* when the rotate angle deviation is 3°. As can be seen, the non-ideal rotate angle results in the crosstalk of the two polarization states, resulting in the decrease of OSSR value. However, the OSSR value can still be guaranteed to be higher than 20 dB when the rotate angle deviation is within 3°, which is acceptable for the system performance.

In actual situations, the phase shift of PS and the rotate angle of PC may deviate simultaneously, which will affect the system performance to a greater extent. In order to discuss the joint influence of these two non-ideal parameters on the quality of the generated signal, we set both the phase deviation and the rotate angle deviation to 3°, then we obtain the 8/12 GHz microwave FSK signal, whose electrical spectrum and waveform are showed in Fig.15 (a) and (b). Compared with Fig.11, we can clearly see that the RFSSR decreases from 22.69dB to 17.50dB due to the increase power of the spurious sideband component at 20GHz, and the waveform has also deteriorated. The reason for this result is that the non-ideal phase shift and non-ideal rotation angle cause the
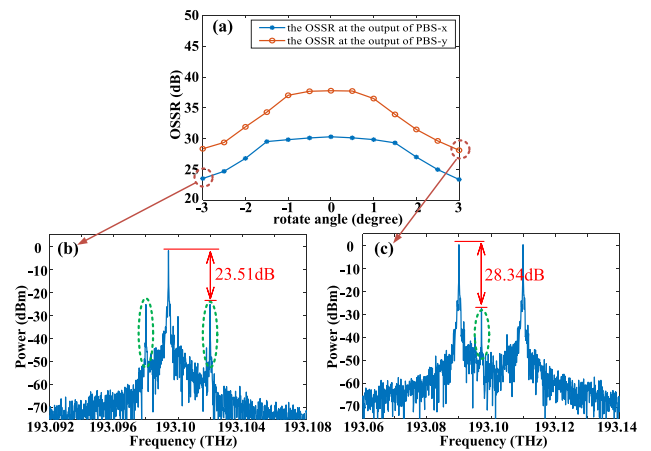

FIGURE 14. (a) the OSSR of the output spectrum at PBS-*x* and PBS-*y* when rotate angle deviation is within 3°. (b) the output optical spectrum at PBS-*x* when the rotate angle is −3°. (c) the output optical spectrum at PBS-*y* when the rotate angle is +3°.
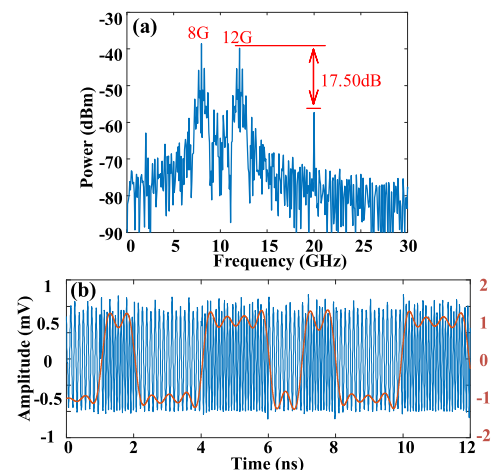

FIGURE 15. (a) the electrical spectrum and (b) the waveform of the generated 1-Gbit/s 8/12 GHz microwave FSK signal when both the phase deviation and the rotate angle deviation are 3°.

increase of the power of the unwanted optical sidebands (as can be seen in Fig. 13 and Fig. 14), which then leads to the power increase of the unwanted frequency components in the electrical spectrum. However, the frequency jump can still be clearly observed and the recovered binary data (red line) is also consistent with the binary coding signal. Then we adjust the frequency of MSG1 from 2GHz to 6GHz by 1GHz steps, and the instantaneous frequency of the generated microwave FSK signal can be obtained, as shown in Fig. 16, in which the subcarriers with different frequencies can also be clearly distinguished. Therefore, as long as the deviation is controlled within 3°, the system performance can be guaranteed.

The DC bias drift is another important non-ideal factor that should be concerned. As we all know, a well-researched and commercialized feed-back bias control technology can be applied to mitigate its impact. However, considering there are many DC biases need to be controlled in the scheme, it is still necessary to investigate the influence of the slight DC
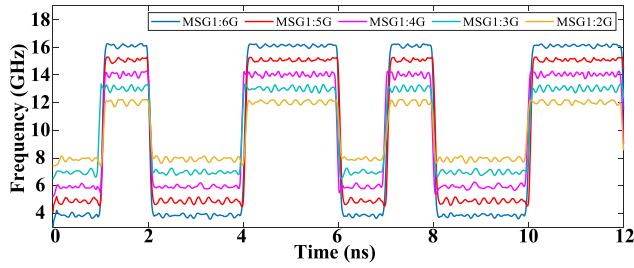
FIGURE 16. The instantaneous frequency of the generated microwave FSK signal at MSG1 frequency of 2/3/4/5/6 GHz when both the phase deviation and the rotate angle deviation are 3°.

TABLE 2. FSK signal with FMF of 2/4.

FSK signal with FMF of 2/4					
V_1	V_2	V_3	V_4	V_5	V_6
0	2.82	4	0	3	2
FSK signal with Tunable Subcarrier Frequencies					
V_1	V_2	V_3	V_4	V_5	V_6
4	4	0	0	-2	4

bias drift on signal quality. In the theoretical analysis, we use φ_i $(i = 1,2,\ldots,6)$ to denote the phase shift introduced by DC bias, and in the simulation work, the corresponding DC bias V_i $(i = 1,2,\ldots,6)$ is given in Table. 2.

Here, we discuss the impact of DC bias drift on the OSSR of the output spectrum of DPMZM$_1$ when the voltage deviation is 0.1V, and the result is shown in Fig.17. Since the V_3 is grounded in actual situations, the drift of V_3 is not considered. As can be seen in Fig.17, the OSSR decreases as the V_1 and V_2 deviate from ideal value 4V, and when V_1 and V_2 are deviate to 3.9V, the OSSR decreases from the maximum value of 30.29dB to 24.6dB, resulting in the deterioration of signal quality. However, since the OSSR is still higher than 24dB, the signal quality can be guaranteed.
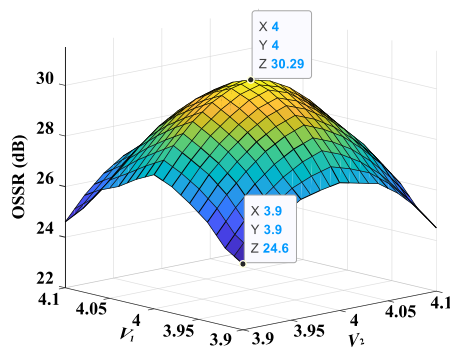

FIGURE 17. The impact of DC bias drift on the OSSR of the output spectrum of DPMZM1 when the voltage deviation is 0.1V.

Likewise, the DC biases may suffer from drift simultaneously, making signal quality worse. In order to observing their joint influence, all non-zero DC biases are set to deviate from the ideal value by 0.1V, i.e., $V_1 = 3.9$V, $V_2 = 3.9$V, $V_3 = -2.1$V and $V_4 = 3.9$V. Fig.18 exhibits the electrical spectrum and waveform of the generated 8/12 GHz microwave
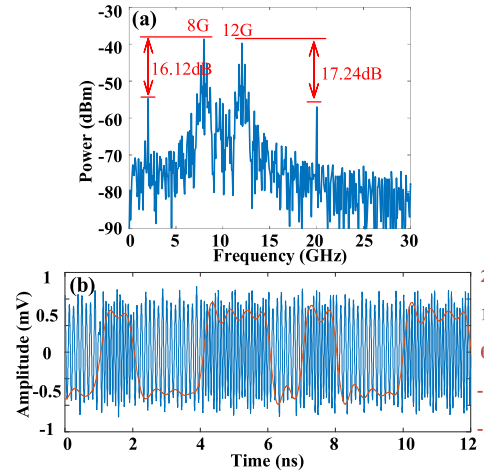

FIGURE 18. (a) the electrical spectrum and (b) the waveform of the generated 1-Gbit/s 8/12 GHz microwave FSK signal when $V_1 = 3.9$V, $V_2 = 3.9$V, $V_3 = -2.1$V and $V_4 = 3.9$V.

FSK signal. Compared with Fig.11, the power of the spurious sideband components at 2GHz and 20GHz are increased and the RFSSR decreases from 22.69dB to 16.12dB. Meanwhile, the waveform has significantly deteriorated. Fortunately, the frequency jump can still be clearly observed and the recovered binary data (red line) is also consistent with the binary coding signal.

In addition, the limited manufacturing process may prevent the time delay τ of OTDL from ideal value, resulting in the unwanted optical sidebands cannot be completely filtered out by TFS. Fig.19 (a) shows the frequency response when τ equals to 25ps, 24.7ps, 24.4ps, 24.1ps. As can be seen, when the time delay τ gradually becomes smaller from the ideal value of 25ps, the frequency response curve will shift to the left and the period will be slightly expanded. Similarly, when the delay is larger than the ideal value, the frequency response curve will shift to the right and the period will be slightly narrowed.
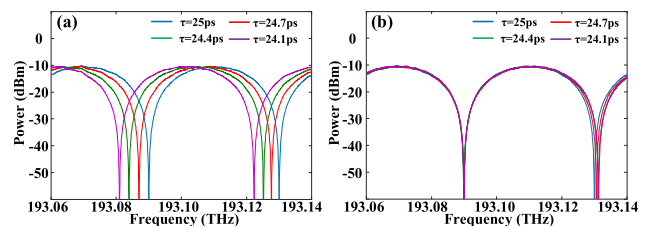

FIGURE 19. (a) the frequency response when τ equals to 25ps, 24.7ps, 24.4ps, 24.1ps. (b) the frequency response after a $\Delta\theta$ compensation.

According to Eq. (7), we can know that a $\Delta\tau$ will cause phase change of the amplitude factor $\cos((\theta + \omega\tau)/2)$, thus making the frequency response curve shift. This problem can be solved by adding a $\Delta\theta$ to compensate the phase change. The $\Delta\theta$ and $\Delta\tau$ should satisfy $(\Delta\theta + \omega\Delta\tau)/2 = k\pi$, (k = 1,2,3$\ldots$). Fig.19 (b) shows the frequency response after a $\Delta\theta$ compensation, where $\Delta\theta = 0.06\pi$ for $\tau = 24.7$ps, $\Delta\theta = 0.12\pi$ for $\tau = 24.4$ps and $\Delta\theta = 0.18\pi$ for $\tau = 24.1$ps.
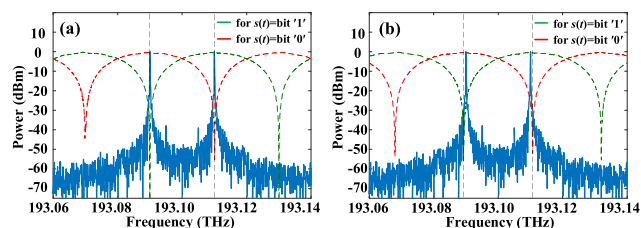
FIGURE 20. (a) the filtering process in TFS when $\tau = 25$ps. (b) the filtering process in TFS when $\tau = 23.5$ps.
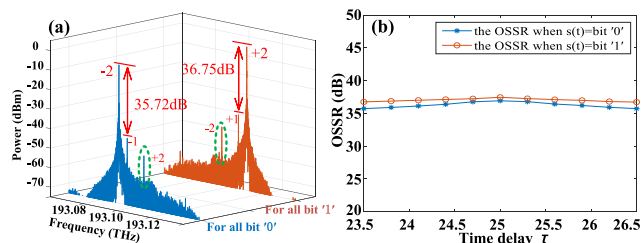

FIGURE 21. (a) the output optical spectrum of the TFS. (b) the OSSR of the output spectrum at TFS when time delay deviation is within 1.5ps.

The filtering process in TFS shows in Fig.20. When $\tau = 25$ps, the optical sidebands are located exactly in the peak/valley of the frequency response curve. And when $\tau = 23.5$ps, the optical sidebands deviate slightly from the peak/valley of the frequency response curve whose period is expanded. Fig.21 (a) shows the output optical spectrum of the TFS. Compared with Fig.10 (b), the OSSR is slightly reduced, and the power of higher-order spurious sideband components (green circle) is increased. However, since the power is still much smaller, their impact on the signal quality is very limited. Fig.21 (b) shows the OSSR of the output spectrum at TFS when time delay τ deviation is within 1.5ps, which can be seen that the value of OSSR almost maintains stable, indicating that the quality of optical signal can be guaranteed.

In practice, the accuracy of a common OTDL can reach the order of ps, and the state-of-art OTDL can reach an order of fs, which makes the influence of non-ideal time delay on signal quality greatly reduced. It is worth mentioning that the time delay τ may suffer from deviation by environmental interference, making the phase compensation difficult and complicated.

Except for the above main non-ideal parameters, there are some other factors may affect the generated signal quality in practical applications, such as the low extinction ratio (ER) of modulators and the amplitude fluctuation of the input electrical signal. Fortunately, some researchers have improved the modulators' structure to achieve more than 50dB ER [21], [22]. In addition, some high extinction ratio (HER) modulators have been commercially available due to the advancement of manufacturing technology. As to the amplitude fluctuation of the input electrical signal, it is highly desired that electronic devices with good performance can be used to generate the binary data and the RF driving

signal in practice. Furthermore, it is noted that the proposed system is polarization-dependent. System performance might be affected due to the variation of the polarization states of the optical signals under the experimental environment. Thereby polarization maintaining fibers is preferred to ensure the system stability. Moreover, polarization state monitor and feedback control could also be utilized to further improve the system stability.

It is worth noting that the structure of our scheme is constructed by discrete components, which makes the system sensitive to environmental interference and thus reduces long-term stability. One solution is to integrate the structure through photonic integrated circuits. Furthermore, thanks to the development of advanced technologies such as silicon-based integration and heterogeneous integration, it is expected to achieve on-chip integrated microwave photonic system, making the large-scale commercialization of microwave photonics possible [23], [24]. By then, most technical solutions will greatly avoid the troubles caused by environmental interference and poor system stability.

IV. CONCLUSION

In summary, we have proposed and investigated a photonic approach to generate multiform microwave FSK signal based on a DP-QPSK modulator and a TFS. A detailed theoretical derivation is conducted to analyze the generation process of microwave FSK signal with frequency multiplication factors of 2/4 and the generation process of microwave FSK signal with tunable subcarrier frequencies. In the simulation work, a 1Gbit/s 10/20GHz microwave FSK signal and a 1Gbit/s 8/12GHz microwave FSK signal are respectively generated, and the frequency tunability are verified, which agree well with the theoretical derivation. In addition, the effects of non-ideal phase value of the PS and non-ideal rotate angle of PC are discussed, and the results show that this scheme has good immunity to the small parameters deviation (within 3°). Compared with the previous works, the proposed scheme realizes multiform microwave FSK signal generation based on a single system, which may find applications in high-frequency multifunction wireless communication system or radar system.

REFERENCES

[1] N. Levanon and I. I. Cohen, "Binary frequency shift keying for continuous waveform radar," *IEEE Trans. Aerosp. Electron. Syst.*, vol. 53, no. 5, pp. 2462–2468, Oct. 2017.

[2] Q. Liu and M. P. Fok, "Ultrafast and wideband microwave photonic frequency-hopping systems: A review," *Appl. Sci.*, vol. 10, no. 2, pp. 521–538, Jan. 2020.

[3] J. Yao, "Microwave photonics," *J. Lightw. Technol.*, vol. 27, no. 3, pp. 314–335, Feb. 1, 2009.

[4] J. Capmany and D. Novak, "Microwave photonics combines two worlds," *Nature Photon.*, vol. 1, no. 6, pp. 319–330, Apr. 2007.

[5] Y. Chen, "High-speed and wideband frequency-hopping microwave signal generation via switching the bias point of an optical modulator," *IEEE Photon. J.*, vol. 10, no. 1, pp. 1–7, Feb. 2018.

[6] P. Cao, X. Hu, L. Zhang, J. Wu, X. Jiang, and Y. Su, "Photonic generation of microwave frequency shift keying signal using a single-drive Mach–Zehnder modulator," *Opt Exp.*, vol. 22, no. 12, pp. 14433–14440, Jun. 2014.

[7] G. Wang, S. Zhao, K. Zhang, T. Lin, X. Li, G. Zhao, and W. Jiang, "Photonic generation of microwave binary modulation signals with high frequency multiplication factors," *Opt. Commun.*, vol. 443, pp. 96–103, Jul. 2019.

[8] L. Huang, P. Wang, P. Xiang, D. Chen, Y. Zhang, J. Tao, T. Pu, and X. Chen, "Photonic generation of microwave frequency shift keying signals," *IEEE Photon. Technol. Lett.*, vol. 28, no. 18, pp. 1928–1931, Sep. 15, 2016.

[9] X. Li, S. Zhao, K. Zhang, Z. Zhu, Y. Zheng, and D. Liang, "Photonic generation of microwave binary digital modulation signal with format agility and parameter tunability," *Opt. Commun.*, vol. 429, pp. 106–111, Dec. 2018.

[10] X. Feng, L. Yan, H. Jiang, P. Li, J. Ye, Y. Zhou, Y. Pan, B. Luo, X. Zou, and T. Zhou, "Photonic generation of multilevel frequency-hopping microwave signal," *IEEE Photon. J.*, vol. 11, no. 1, pp. 1–7, Feb. 2019.

[11] X. Feng, L. Yan, P. Li, J. Ye, X. Zou, W. Pan, and B. Luo, "Photonic approach for generation and fast switching of binary digitally modulated RF signals," *IEEE Photon. J.*, vol. 12, no. 5, pp. 1–8, Oct. 2020.

[12] M. Lei, Z. Zheng, C. Song, Y. Bai, J. Qian, S. Huang, and X. Gao, "Equivalent photonic switch for microwave frequency shift keying signal generation," *Opt Lett*, vol. 44, no. 12, pp. 3138–3141, Jun. 2019.

[13] J. Ye, L. Yan, H. Wang, W. Pan, B. Luo, and X. Zou, "Photonic generation of microwave frequency shift keying signal using a polarization maintaining FBG," *IEEE Photon. J.*, vol. 10, no. 3, pp. 1–8, Jun. 2018.

[14] Y. Xie, L. Zhuang, P. Jiao, and D. Dai, "Sub-nanosecond-speed frequency-reconfigurable photonic radio frequency switch using a silicon modulator," *Photon. Res.*, vol. 8, no. 6, p. 852, Jun. 2020.

[15] W. Zhai, A. Wen, and K. Wei, "Photonic generation of a dual-band polyphase-coded microwave signal with a tunable frequency multiplication factor," *J. Lightw. Technol.*, vol. 37, no. 19, pp. 4911–4920, Oct. 1, 2019.

[16] Y. Chen, A. Wen, and W. Zhang, "Generation of phase-coded microwave signals through equivalent phase modulation," *IEEE Photon. Technol. Lett.*, vol. 29, no. 16, pp. 1371–1374, Aug. 15, 2017.

[17] J. Shi, F. Zhang, D. Ben, and S. Pan, "Simultaneous radar detection and frequency measurement by broadband microwave photonic processing," *J. Lightw. Technol.*, vol. 38, no. 8, pp. 2171–2179, 2020.

[18] K. Zhang, S. Zhao, X. Li, Z. Zhu, W. Jiang, T. Lin, and G. Wang, "Photonic approach to dual-band dual-chirp microwave waveform generation with multiplying central frequency and bandwidth," *Opt. Commun.*, vol. 437, pp. 17–26, Apr. 2019.

[19] Z. Zhu, S. Zhao, X. Li, K. Qu, and T. Lin, "Frequency-doubled microwave waveforms generation using a dual-polarization quadrature phase shift keying modulator driven by a single frequency radio frequency signal," *Opt. Laser Technol.*, vol. 98, pp. 304–397, Jan. 2018.

[20] T. Lin, S. Zhao, Z. Zhu, X. Li, Q. Zheng, K. Qu, and D. Hu, "Microwave photonic image rejection mixer based on a DP-QPSK modulator," *J. Modern Opt.*, vol. 64, no. 17, pp. 1699–1707, Sep. 2017.

[21] Y. Yamaguchi, S. Nakajima, H. Nakajima, M. Izutsu, A. Kanno, and T. Kawanishi, "Single mach-zehnder modulator with active Y-branch for higher than 60 dB extinction-ratio operation," in *Proc. 39th Eur. Conf. Exhib. Opt. Commun. (ECOC)*, 2013, pp. 1–3.

[22] Y. Ogiso, Y. Tsuchiya, S. Shinada, S. Nakajima, T. Kawanishi, and H. Nakajima, "High extinction-ratio integrated Mach–Zehnder modulator with active Y-branch for optical SSB signal generation," *IEEE Photon. Technol. Lett.*, vol. 22, no. 12, pp. 941–943, Jun. 2010.

[23] G. Carpintero, R. C. Guzman, A. Zarzuelo, J. Cesar, M. Ali, and M. C. Lo, "Integrated microwave photonics: The path to high quality millimeter and terahertz wave signal generation?" in *Proc. IEEE Photon. Conf. (IPC)*, Sep. 2019, pp. 1–2.

[24] W. Zhang and J. Yao, "Silicon-based integrated microwave photonics," *IEEE J. Quantum Electron.*, vol. 52, no. 1, pp. 1–12, Jan. 2016.
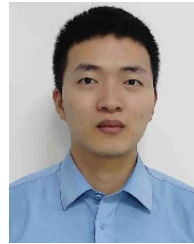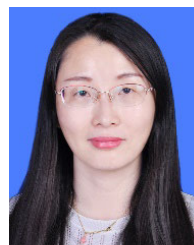
GUODONG WANG received the B.S. and M.S. degrees from Air Force Engineering University, Xi'an, China, in 2017 and 2020, respectively, where he is currently pursuing the Ph.D. degree. His research interests include microwave photonics and microwave signal processing

KUISHENG FENG received the B.S. and M.S. degrees from Air Force Engineering University, in 2002 and 2006, respectively, and the Ph.D. degree in electromagnetic field and microwave technology from Northwestern Polytechnical University (NPU), Xi'an, in 2011. From 2011 to 2014, he was engaged in Postdoctoral Research with Northwestern Polytechnical University. He is currently an Associate Professor with the College of Artificial Intelligence, Yango University. His research interests include satellite communications antennas, ultra-wideband and high gain antennas, electromagnetic metamaterials, the broadband and reconfigurable perfect metamaterial absorber, and its application for RCS reduction of antennas.

XUAN LI received the B.E., M.E., and Ph.D. degrees from the School of Information and Navigation, Air Force Engineering University, Xi'an, China, in 2011, 2014, and 2017, respectively. From March 2015 to June 2016, he was with the Microwave Photonics Research Laboratory, College of Electronic and Information Engineering, Nanjing University of Aeronautics and Astronautics, Nanjing, China. He is currently a Teacher with Air Force Engineering University. His current research interests include arbitrary waveform generation and signal processing.

WEI JIANG received the bachelor's and master's degrees from Air Force Engineering University, Xi'an, China, in 2004 and 2007, respectively, where she is currently pursuing the Ph.D. degree. She is also a Senior Engineer with the National Key Laboratory of Science and Technology on Space Microwave, Xi'an. Her research interests include optical satellite networks, on-board optical signal processing, and microwave photonics.

NA LI received the M.S. and Ph.D. degrees from Air Force Engineering University, in 2007 and 2012, respectively. She is currently an Associate Professor with the College of Artificial Intelligence, Yango University. Her research interests include quantum communication, network security, and secure communications.

ZONGFENG LI received the B.S. degree from the Electronic Science and Technology Department, Fujian Agriculture and Forestry University, in 2006. He is currently an Engineer with the College of Artificial Intelligence, Yango University. His research interests include circuit analysis and digital circuit.

• • •